Materials Science and Engineering C 67 (2016) 717–726

Contents lists available at ScienceDirect

Materials Science and Engineering C

journal homepage: www.elsevier.com/locate/msec

Design of chitosan-based nanoparticles functionalized with gallic acid

J. Lamarra [a,b], S. Rivero [a,b], A. Pinotti [a,c,*]

[a] Center for Research and Development in Food Cryotechnology (CCT-CONICET La Plata), 47 and 116, La Plata 1900, Argentina
[b] Faculty of Exact Sciences, UNLP, Argentina
[c] Faculty of Engineering, UNLP, Argentina

ARTICLE INFO

Article history:
Received 17 February 2016
Received in revised form 24 April 2016
Accepted 16 May 2016
Available online 18 May 2016

Keywords:
Central composite design
Zeta potential
Percentage encapsulation efficiency
QuickScan
Ionotropic gelation
RSM

ABSTRACT

Active nanoparticles based on chitosan could be applied as a support for the modulation of gallic acid delivery. In this sense, these nanostructures could be employed in different fields such as food, packaging, and pharmaceutical areas. The design parameters of chitosan-based nanoparticles functionalized with gallic acid (GA) were optimized through RSM by means of the analysis of zeta potential (ZP) and percentage encapsulation efficiency (PEE). The nanoparticles were prepared by ionotropic gelation using tripolyphosphate (TPP), at different combinations of chitosan (CH) concentration, CH:TPP ratio and GA. Global desirability methodology allowed finding the optimum formulation that included CH 0.76% (w/w), CH:TPP ratio of 5 and 37 mg_{GA}/g_{CH} leading to ZP of +50 mV and 82% of PEE.

Analysis through QuickScan and turbidity demonstrated that the most stable nanoparticle suspensions were achieved combining concentrations of chitosan ranging between 0.5 and 0.75% with CH:TPP ratios higher than 3. These suspensions had high stability confirmed by means ZP and transmittance values which were higher than +25 mV and 0.21 on average, respectively, as well as nanoparticle diameters of about 140 nm.

FTIR revealed the occurrence of both hydrogen bond and ionic interactions of CH-TPP which allowed the encapsulation and the improvement of the stability of the active agent.

1. Introduction

Research and the application of polyphenols have recently attracted a great interest in the functional foods, nutraceutical, and pharmaceutical industries, due to their potential health benefits to humans. Gallic acid (GA, 3, 4, 5-trihydroxybenzoic acid) is found in abundance in the plant kingdom, especially in tea, grapes, berries, and other fruits, as well as in wine. This polyphenol exhibits a variety of biochemical properties, as antioxidant, antimicrobial, and anti-inflammatory, and it has anticancer and neuroprotectant effects [1]. GA has high reducing potential and scavenging properties toward radical species which explains its antioxidant capacity [2,3]. These functions make it widely used in foods, drugs, and cosmetics [4,5].

The inclusion of polyphenol extracts more concentrated than naturally present in foods is hindered due to off-flavors, poor stability, and reduced solubility. In this context, the use of encapsulation technology has helped overcome these issues by entrapping the phenolic compounds within biopolymer carriers to better control the dosage, improve their stability against oxidation, provide site-specific targeted delivery, mask off-flavors, and improve their miscibility in aqueous food products [6].

The appearance of the nanotechnology has triggered enormous possibilities for obtaining innovative products such as nanosensors [7–9] and applications for a wide spectrum of nutraceutical and food consumption sectors. On the other hand, Patel et al. [10] and Pinheiroa et al. [11] evaluated the abilities of biopolymeric matrices to provide remarkable protection the incorporated compounds against thermo- or photo-degradation.

Chitosan is increasingly favored in various fields of drug delivery. From the chemical point of view, it is a polycationic copolymer consisting of β-(1–4)-linked glucosamine and N-acetylglucosamine units, soluble in an acidic environment due to protonation of the amino groups. The presence of reactive amino groups means that chitosan can be modified easily to create and nanoparticles or porous hydrogels. The resultant positive charge makes it possible to prepare nanoparticles by ionotropic gelation with multivalent anions, such as tripolyphosphate (TPP) [12].

The interaction of chitosan with TPP leads to the formation of biocompatible cross-linked chitosan nanoparticles. The cross-linking density, crystallinity, and hydrophilicity of cross-linked chitosan allow modulation of drug release and extend its range of potential applications in drug delivery based on nanocapsule design. Probably due to a more compact structure, the complex nanoparticles were found to provide additional protection the embedded compounds against heat or light-induced degradation [13]. Chitosan has been reported extensively as an encapsulant for bioactive compounds, such as vitamins and minerals [14–16], catechins [17] and proteins [18].

* Corresponding author.
E-mail address: acaimpronta@hotmail.com (A. Pinotti).

http://dx.doi.org/10.1016/j.msec.2016.05.072
0928-4931/

Further, antioxidant-chitosan conjugates showed diverse bioactivities, including antioxidant, anticancer, and inhibitory effects on digestive enzymes, β-secretase, and food-borne pathogens [4].

Experimental design consists of a set of experiments, in which the levels of all contributing variables are changed simultaneously in a systematic manner. The traditional one-factor at a time (OFAT) technique used for optimization does not take into account interactions between the factors and provides less information about the variability of the response [19]. In contrast, the experimental design is a valuable tool for measuring interactions among factors and for the prediction of optimal conditions, being less expensive and less time-consuming [20]. Another strong point of using statistical optimization is that no complex calculations are required to analyze the resulting data [21].

A central composite design (CCD) consists of embedded factorial design, star points to estimate the curvature, and center points to evaluate the experimental reproducibility. The center points are selected to obtain several properties, such as rotatability or orthogonality, in order to fit the quadratic polynomials [22]. This statistical tool significantly reduces the number of empirical experiments that are necessary to identify a mathematical trend in the experimental design, facilitating determination of the optimum level of variable factors required for a given response [23]. The CCD is one of the designs most used, due to its flexibility. It has been successfully applied to the optimization of many bioprocesses [24,25].

Among different types of experimental design, the response surface methodology (RSM) has become the standard approach for many of the experiments carried out for optimization purposes. RSM is mostly concerned with approximating a complex, unknown function with a polynomial, usually either a first-order model or a second-order model. Consequently, designs for fitting these models are of considerable interest and allow estimating interaction and even quadratic effects and therefore, give us an idea of the shape of the response surface.

There is hardly any information about the optimization of the nanoencapsulation process of food preservatives by using chitosan matrices. In this sense, this study seeks to contribute to the food preservation by means useful information about tailor-made functionalized nanoparticles. Therefore, the objectives of the present work were: to a) optimize design parameters for encapsulating GA in chitosan particles by using RSM focusing on food applications, b) evaluate the effects of key processing variables (chitosan concentration, CH:TPP ratio and GA concentration) on the yield of the functionalizated nanoparticles through zeta potential and percentage encapsulation efficiency, c) evaluate the physical suspension stability by means of QuickScan and turbidity methods, d) obtain information concerning the way by which the components of the particle system interact among them through FTIR.

2. Materials

Chitosan (CH) from crab shells with a minimum deacetylation degree of 85% and a molecular weight of 4.8×10^5 Da was purchased from Polymar Ciência e Nutrição (Fortaleza, Brazil). Analytical grade sodium tripolyphosphate (TPP), gallic acid (GA) and acetic acid were supplied by Anedra (Buenos Aires, Argentina).

3. Methods

3.1. Preparation of nanoparticles

A stock chitosan solution of 2% (w/w) was prepared by solubilization in 2% (v/v) acetic acid solution at 20 °C under continuous stirring for 24 h approximately, followed by a vacuum filtration to eliminate insoluble materials. Cross-linking agent sodium tripolyphosphate was dissolved in distilled water under constant stirring at the concentration of 2% (w/v) to prepare the stock TPP solution. CH and TPP solutions of different concentrations were obtained from the stock solutions consistent with the concentrations summarized in Table 1. Afterwards, the corresponding amounts of GA were added to the carrier solutions until reaching the final concentration (expressed as mg per gram CH) as shown in Table 1.

The CH nanoparticles were obtained by inducing the ionotropic gelation of a chitosan solution using TPP as counter ion, following the method described by Calvo et al. [26] with some modifications. Nanoparticles were formed spontaneously by dropwise addition of a TPP solution into a solution containing CH and GA. Once this process was completed, the obtained suspensions were homogenized at 13,500 rpm for 10 min by means of an Ultraturrax T-25 (Janke & Kunkel, IKA-Labortechnik, Germany).

From here onwards, the chitosan nanoparticles charged with GA will be called F_1, F_2, …, F_n, with $n = 15$.

3.2. Percentage encapsulation efficiency (PEE)

To determine the percentage encapsulation efficiency, the synthesized nanoparticles were separated from the suspension by centrifugation at 20.000 rpm for 20 min (Beckman Coulter Optima L-100XP Floor Centrifugation System, California, USA). Samples were filtered using 0.45 μm sterile nylon (Millipore, Bedford, MA, USA) and the concentration of GA was quantified by using a Spectrophotometer DU 650 (Beckman, USA) [5]. The concentration of the active agent in both the supernatant and the precipitate was calculated according to a calibration curve, prepared by measuring the absorbance at $\lambda = 269$ nm (determined as the maximum of absorbance of the active compound) of known concentrations of GA. The calculated concentration was then multiplied by the volume of the supernatant to determine the total amount of GA present in the supernatant. All the measures were carried out by triplicate.

The PEE percentage was determined as follows:

$$\mathrm{PEE} = \frac{W_i - W_s}{W_i} \times 100 \quad (1)$$

where, W_i is the mass of GA used for preparation of the nanoparticles and W_s is the mass of GA measured in the supernatant.

3.3. Zeta potential, particle sizes and polydispersity index

Zeta potential and particle hydrodynamic size of the nanoparticle suspensions were determined by dynamic laser light scattering by using a Zetasizer Nano-ZS instrument (Malvern Instruments, Worcestershire, England) provided with a He—Ne laser beam operating at 633 nm at a fixed scattering angle of 173° and a digital correlator Model ZEN3600. ZP was determined by measuring the direction and velocity of droplet movement in a well defined electric field. Prior to the analysis, the index of refraction, determined by using a digital refractometer (Atago, USA), and the conductivity, measured with a pH/conductivity meter (Mettler Toledo Urdorf, Switzerland), were evaluated in each and every suspension.

The zeta potential was reported as the average and standard deviation of measurements made on two samples, performing five determinations per sample.

Polydispersity index (PDI) is a parameter to define the nanoparticle size distribution obtained from photon correlation spectroscopic analysis. It is a dimensionless number extrapolated from the autocorrelation function and ranges from a value of 0.01 for monodispersed particles up to values of 0.5–0.7. Samples with very broad size distribution have PDI values >0.7 [27,28].

3.4. Response surface methodology

The major factors affecting the particle size and percentage encapsulation efficiency of nanoparticles were the biopolymer concentration of CH, the active agent concentration GA and the ratio of the biopolymer to the crosslinking agent CH:TPP.

Table 1
Central composite design (CCD) of three independent variables at different levels and both observed responses: zeta potential (ZP) and percentage encapsulation efficiency (PEE). Actual and codified variables were: chitosan concentration (w/w), chitosan:tripolyphosphate ratio (CH:TPP) and gallic acid concentration expressed as mg_{GA}/g_{CH}, according to the selected design.

	CH	CH:TPP	GA/g_{CH}	CH (%)	CH:TPP	GA (mg/g_{CH})	Observed responses	
Formulation (F_n)	Coded variables			Actual variables			ZP (mV)	PEE
1	−1	−1	−1	0.5	1.81	25	11.0 (1.0)[a]	74.9 (3.3)[a]
2	−1	−1	1	0.5	1.81	75	9.7 (1.3)[a]	83.9 (3.3)[b]
3	−1	1	−1	0.5	4.19	25	36.4 (1.9)[d]	83.4 (2.7)[b,d]
4	−1	1	1	0.5	4.19	75	39.2 (2.1)[d]	83.3 (2.7)[b,d]
5	1	−1	−1	1	1.81	25	9.3 (1.1)[a]	59.5 (2.9)[c]
6	1	−1	1	1	1.81	75	8.9 (0.7)[a]	73.6 (3.1)[a]
7	1	1	−1	1	4.19	25	48.1 (4.0)[e]	74.3 (3.5)[a]
8	1	1	1	1	4.19	75	46.7 (3.6)[e]	68.3 (2.7)[b]
9	1.682	0	0	0.33	3	50	23.9 (1.2)[b]	83.9 (2.6)[b]
10	1.682	0	0	1.17	3	50	27.8 (2.1)[c]	64.1 (3.1)[c]
11	0	−1.682	0	0.75	1	50	5.3 (0.6)[a]	70.9 (3.3)[a,e]
12	0	1.682	0	0.75	5	50	46.6 (3.2)[e]	80.9 (2.1)[b,d]
13	0	0	−1.682	0.75	3	8	26.0 (1.8)[b,c]	65.5 (3.8)[c,e]
14	0	0	1.682	0.75	3	92	22.2 (0.7)[b]	73.2 (3.4)[a,e]
15	0	0	0	0.75	3	50	27.7 (1.2)[b,c]	80.4 (1.8)[d]
16	0	0	0	0.75	3	50	25.9 (1.5)[b,c]	79.5 (2.0)[d]
17	0	0	0	0.75	3	50	27.5 (1.4)[b,c]	79.6 (2.4)[d]
18	0	0	0	0.75	3	50	28.4 (1.3)[b,c]	79.4 (1.9)[d]

The values in parentheses correspond to the standard deviation.
[a,b]Different letters in the same column indicate significant differences ($P < 0.05$) between samples.

The optimization of the processes was carried out by using an experimental design through RSM. A Central Composite Design with 3 factors and 3 levels was used with 14 experiments and the center point replicated four times [29]. Table 1 shows the actual and codified concentrations, the factors being CH, CH:TPP and GA varied from 0.33 to 1.17%, 1 to 5 and 8 to 92 mg_{GA}/g_{CH}, respectively.

The three-dimensional graphical representation of the system behavior, called the response surface, was used to describe the interaction effects of the variables on the ZP and PEE. These responses were the results of the individual influence and the interactions of the three independent variables.

To predict the optimal conditions, a second-order polynomial function was fitted to the correlate relationship between the independent variables and the response. For three factor levels, the following equation was obtained:

$$y = \beta_0 + \beta_1 x_1 + \beta_2 x_2 + \beta_3 x_3 + \beta_{11} x_1^2 + \beta_{22} x_2^2 + \beta_{33} x_3^2 + \beta_{12} x_1 x_2 + \beta_{13} x_1 x_3 + \beta_{23} x_2 x_3 \quad (2)$$

where, y is the response as a function of x_1, x_2 and x_3, codified independent variables, β_0 is a constant term, β_1, β_2 and β_3 are the coefficients of linear terms, β_{11}, β_{22} and β_{33} are the coefficients of quadratic terms, and β_{12}, β_{13} and β_{23} are the coefficients of interaction effects.

The four replicates (runs 15 to 18) of the center point (15) were carried out in order to estimate the pure error variance [30].

After model fitting was achieved, residual analysis was conducted to validate the assumptions used in the analysis of variance and to identify outliers, examining diagnostic plots such as residual plots. The proportion of variance explained by the models obtained was given by the multiple coefficient of determination, R^2 and the adjusted coefficient of determination (R^2_{adj}) whereas the adequacy of the model was determined by a lack of fit test.

All statistical analysis, generation of response surfaces, desirability functional analysis, optimization, 3D and contour plots were accomplished by using the Expert Design (trial version 7.1.6, Stat-Ease Inc., Minneapolis, USA) statistical software.

In order to minimize the influence of unexplained variability in the responses, the experiments were randomized. The results of these experiments were compared using analysis of variance (ANOVA) (SYSTAT, Inc., Evanston, IL, USA), which was able to determine if the factors and the interactions between factors were significant. Experimental data were reported as mean values with the corresponding standard deviation given between parentheses when appropriate. For simultaneous pairwise comparisons, least significant differences (LSD) test was chosen. Differences in means and F-tests were considered significant when $P < 0.05$.

3.5. Suspension stability

The global stability of the suspensions was carried out by light scattering with a vertical scan analyzer (QuickScan, Beckman Coulter, Fullerton, USA) at room temperature. The suspensions were placed in a cylindrical glass cell, and scanned from the bottom to the top with a monochromatic light source ($\lambda = 850$ nm) as a function of the height of the sample tube (ca. 65 mm) in quiescent conditions, acquiring Transmittance and BS each 40 m (1620 acquisitions in each scan).

In this way, the physical evolution of this process was followed without disturbing the original system and with good accuracy and reproducibility [31,32].

In this method, two synchronized optical sensors recorded simultaneously, the light transmitted (T) through the sample (0° from the incident light), and light backscattered (BS) by the sample (135° from the incident radiation). These data are represented in curves of Transmittance and/or Backscattering (%) as a function of the tube height (mm). From the recorded profiles, mean values of the transmission, in the 20–50 mm zone corresponding to the medium part of the tube, were obtained. Measurements were performed at least in duplicate.

3.6. Optical properties

The transmittance of the nanoparticle suspensions was measured at room temperature (25 °C) with a Beckman DU650 spectrophotometer (Palo Alto, CA, USA) at a wavelength (λT) of 500 nm.

In this way, the turbidity (τ) of a suspension of particles is a measure of the reduction in intensity of the transmitted beam due to scattering and can be calculated from the transmittance using the Lambert–Beer law.

The turbidity is defined by Melik and Fogler [33] and Jonassen et al. [12] as follows:

$$A = -\log T = -\log \frac{I}{I_0} \quad (3)$$

$$\tau = \frac{1}{l} \ln\left(\frac{I_0}{I}\right) = \frac{1}{l} A \times 2.303 \quad (4)$$

where, l is the scattering path length in the sample cell (1.0 cm quartz cuvette) and, I_0 and I are the intensities of the incident and transmitted beams, respectively.

3.7. FTIR spectroscopy

Samples to be tested by FTIR consisting in CH, CHGA and nanoparticles loaded with GA. Film of CH 0.75% (w/w) and chitosan with the addition of 50 mg_{GA}/g_{CH} (CHGA) solutions were obtained by casting and drying at 37 °C in an oven until reaching a constant weight. In addition, suspensions of CHTPP functionalized with GA in accordance with the formulations presented in Table 1 were centrifuged, washed and resuspended. After that, they were casted and dried at 37 °C in order to obtain the corresponding films.

The Fourier transform infrared (FTIR) spectra of the thin films aforementioned were recorded in an IR spectrometer (Nicolet, iS10 Thermo Scientific, Madison, USA) in the wavenumber range 4000–400 cm^{-1} by accumulation of 64 scans at 4 cm^{-1} resolution. Data were analyzed by using the software Omnic 8 (Thermo Scientific).

3.8. Morphological characterization by TEM

The morphological characteristics of the nanoparticles were examined by using a transmission electron microscope (JEM 1200EX II Jeol, Japan) equipped with a digital camera (ES500W Erlangshen CCD Gatan). Briefly, a drop of the suspension was placed on a pretreated copper grid, which was coated with an amorphous thin carbon film. The excess solution was removed by blotting with a filter paper and dried at room temperature. The nanoparticles were collected by centrifugation (Beckman Coulter Optima L-100XP Floor Centrifugation System) at 20,000 rpm for 20 min. The supernatants were discarded, and the particles were washed several times with distilled water, and redispersed in an aqueous medium. Samples were appropriately diluted with distilled water prior to measurement.

4. Results and discussion

4.1. Preparation of CH:TPP nanoparticles

Chitosan has a rigid crystalline structure through inter- and intramolecular hydrogen bonds. In acetic acid solutions chitosan molecules assume an extended conformation owing to the electrostatic charge repulsion between the chains. Nanoparticles can be prepared by the ionic gelation technique because of the opposite charges of CH and TPP. When chitosan and TPP were mixed with each other, they spontaneously formed nanoparticles with an overall positive surface charge [12,34].

It is noteworthy that the stability, determined by the physicochemical features of these suspensions, could be affected as a result of the interaction between of nanoparticles loaded. Consequently, the effects of CH concentration, CH:TPP ratio and GA amount on the stability were analyzed throughout ZP, PEE, nanoparticle sizes, QuickScan and turbidity measures.

4.2. Response surface methodology

Response surface methodology (RSM) has been reported to be an effective tool for optimizing a process when the independent variables have a combined effect on the desired response [35].

The quadratic model was found to be significant with an F_{ZP} value of 241.28 and F_{PEE} value of 37.86 ($P < 0.0001$), which indicated that responses ZP, PEE and the set of independent variables (CH, CH:TPP, GA) were significantly related among them.

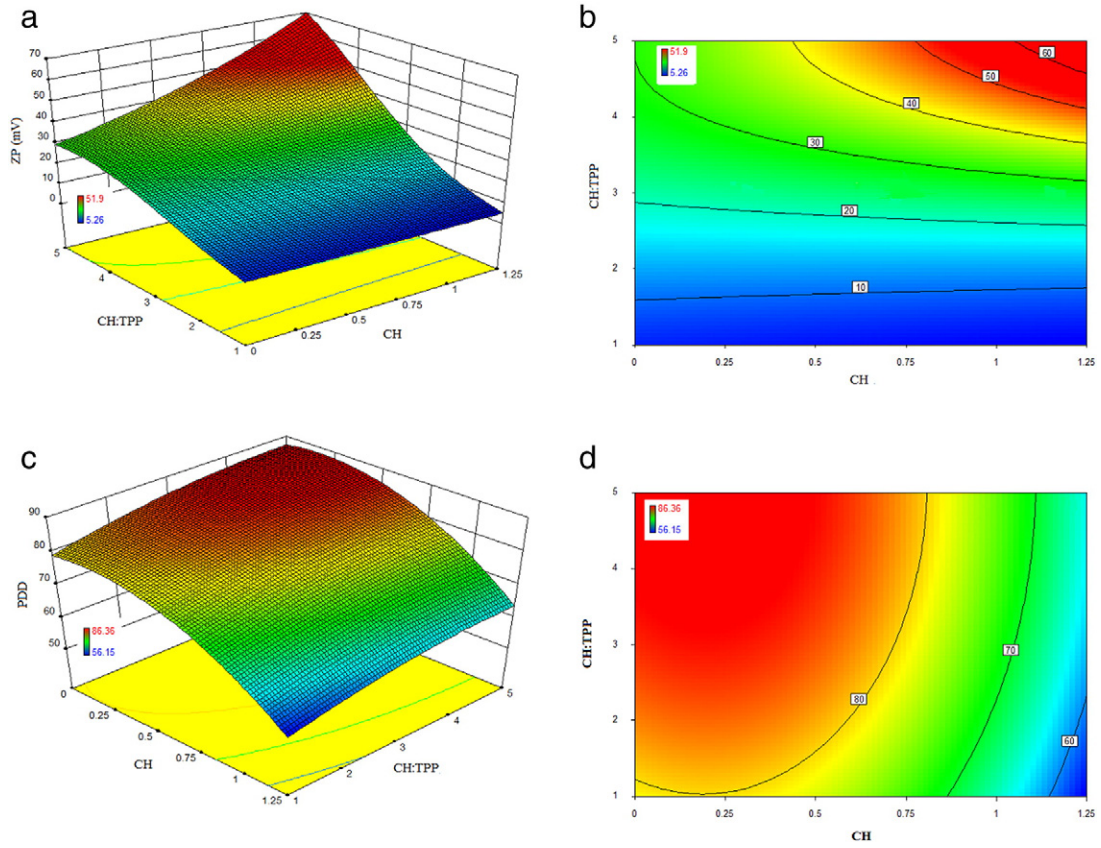

Fig. 1. Response surface of: a) Zeta potential (ZP) and c) Percentage encapsulation efficiency (PEE) and contour plot of: b) ZP and d) PEE as a function of chitosan concentration and CH:TPP ratio, expressed as codified values. The color scale is indicated in each Figure and lines correspond to isoparametric values.

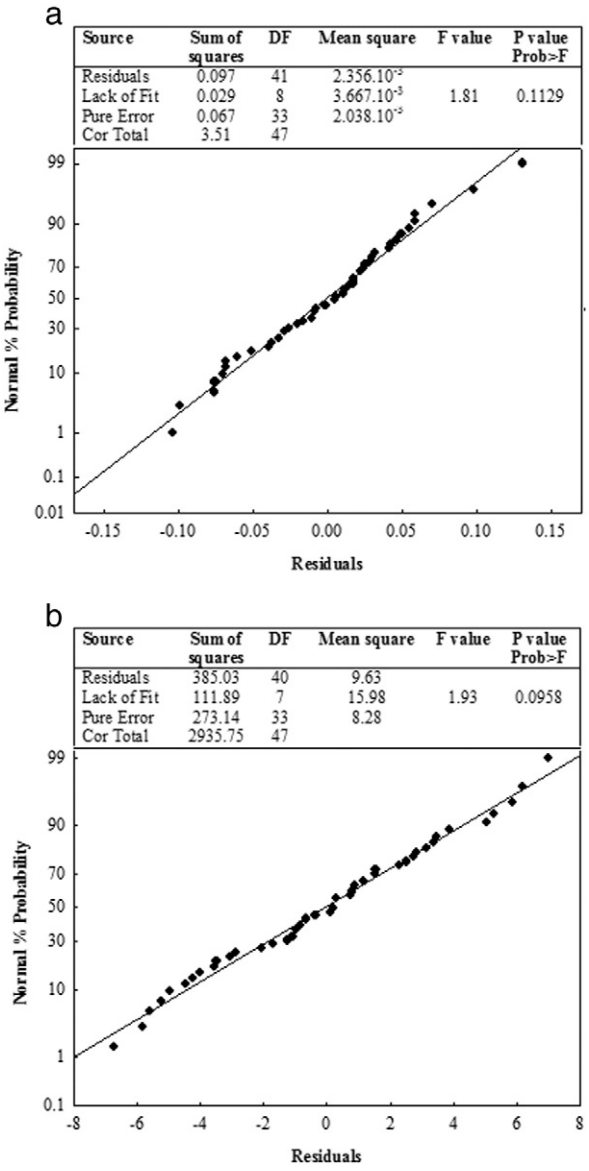

Fig. 2. Normal percent probability of residuals for: a) zeta potential (ZP) and b) percentage encapsulation efficiency (PEE). Tables insert in each Figure show that the lack of fit was non-significant for both analyzed responses.

Concerning zeta potential, a log transformation was required because of the ratio of maximum to the minimum value was higher than 10. Generally, transformations are used for stabilizing the response variance, making the distribution of the response variable closer to the normal distribution, and improving the fit of the model to the data [41].

Applying the multiple regression analysis to output ZP data, the quadratic equation, in which the non-significant (CH × GA), (CH:TPP × GA) interactions and $(CH)^2$ term were removed, allowed the best fit (of these data).

The regression model in terms of both, coded and actual variables was as follows:

$$Log_{10}(ZP) = 1.42 + 0.025 \times x_1 + 0.28 \times x_2 - 0.012 \times x_3 + 0.03 \times (x_1 \times x_2) - 0.070 \times {x_2}^2 - 0.019 \times {x_3}^2 \quad (5)$$

$$Log_{10}(ZP) = 0.37 - 0.020 \times CH - 0.45 \times CH:TPP + 2.61.10^{-3} \times GA + 0.099 \times (CH \times CH:TPP) - 0.049 \times (CH:TPP)^2 - 3.08.10^{-5} \times (GA)^2 \quad (6)$$

According to Ramadan et al. [36], the determination of ZP is a measure of the diffuse layer thickness. The higher the ZP value, the thicker the diffuse layer, and the more stable the suspension is. For low molecular weight surfactants and pure electric stabilization, absolute ZP values above 30 mV indicate good stability of the suspension and above 60 mV provide excellent stability [36–38]. On the other hand, for large molecular weight stabilizers which act mainly by steric stabilization, ZP values of only 20 mV or much lower can provide sufficient stabilization. This behavior is because of the fact that the adsorbed layers of large molecular weight stabilizer shift the plane of shear to a farer distance from the particle surface and consequently lead to a ZP value decrease [36]. Other authors, working on CH-based nanoparticles, found ZP in a similar range of values [39,40].

For CH solution, the zeta potential value was + 58 mV which was associated with the positively charged amine groups at acidic pH. Chitosan is a compound which combines the electrostatic stabilization due to its positive charge, and the steric stabilization because of its polymeric nature. In the same way, the zeta potential of the nanoparticles was always positive indicating the presence of amino groups of chitosan on the surface [12]. As shown in Fig. 1a, the ZP of the nanoparticles increased with increasing CH:TPP ratio, this increase being more marked when CH concentration was higher than about 0.5% [28]. The extreme ZP values were obtained because of the interaction term (CH × CH:TPP).

Loaded nanoparticles gave ZP values lower as TPP concentration increased because of the neutralization of the CH positive charges. Instead, there was no significant effect of GA concentration on ZP value. This fact

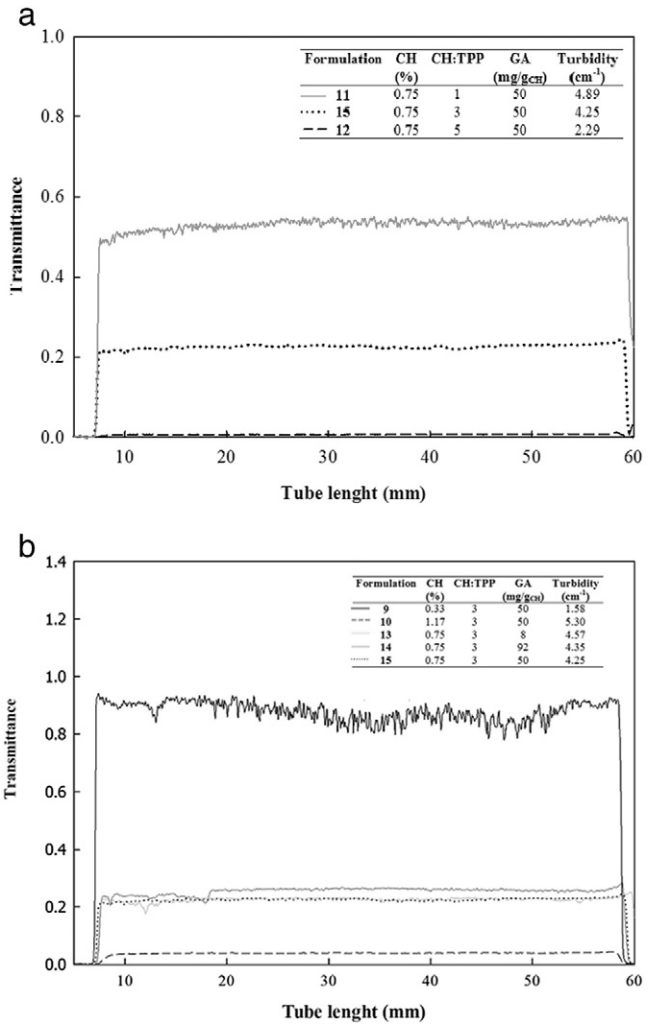

Fig. 3. Transmittance profiles obtained by QuickScan method of samples: a) F_{11}, F_{15} and F_{12} formulated with 0.75% CH, 50 mg_{GA}/g_{CH} and CH:TPP ratios of 1, 3 and 5, respectively; b) F_9, F_{10}, F_{13}, F_{14} and F_{15} prepared with a constant CH:TPP ratio of 3.

could be explained owing to the small amount of GA used in these experiments.

Points located on contour line corresponding to ZP + 30 mV were obtained with CH:TPP ratios higher than about 3.5 irrespective of CH concentration (Fig. 1b). Meanwhile, ZP higher than +40 was achieved only combining CH:TPP ratios higher than 4 with CH concentrations ranging between 0.5 and 1.25%. The lowest values of the response were obtained for CH:TPP ratios smaller than 3 regardless of the CH concentration.

On the other hand, considering output percentage encapsulation efficiency data, the quadratic equation also permitted the best fit, removing the non-significant (CH × CH:TPP), (CH × GA) interactions.

The expressions in terms of both, coded and actual variables were the following:

$$PEE = 79.22 - 6.08 \times x_1 + 2.51 \times x_2 + 2.18 \times x_3 - 3.65 \times (x_2 \times x_3) - 1.35 \times x_1^2 - 0.69 \times x_2^2 - 3.0 \times x_3^2 \quad (7)$$

$$PEE = 39.84 + 8.14 \times CH + 11.16 \times CH:TPP + 0.93 \times GA - 0.12 \times (CH:TPP \times GA) - 21.64 \times (CH)^2 - 0.49 \times (CH:TPP)^2 - 0.49.10^{-3} \times (GA)^2 \quad (8)$$

When the lower the CH concentration and the higher the CH:TPP ratio were, the higher the PEE obtained (Fig. 1c). This result suggested that the complex nanoparticles possessed a more compact structure, with more functional groups involved in the polymer–active agent interaction. Although, CH:TPP × GA interaction diminished the PEE, GA concentration practically did not have an effect on this response.

As can be seen in Fig. 1d, PEE contour line corresponding to 80% was obtained with CH concentration ranging between 0.5 and 0.75% (w/w) combined with CH:TPP ratio of about 1.5 and 4, respectively. It is worth mentioning that PEE higher than 85% was achieved while CH concentration did not exceed 0.6% (w/w) and CH:TPP ratio was higher than 4. That would mean the encapsulation process is strongly dependent on positive charge of the encapsulant (polymer).

The residual analysis is one method to corroborate the model adequacy. The check of the normality assumption was made by constructing a normal probability plot of the residuals, as depicted in Fig. 2a and b. The normality was satisfactory as all residual plots were distributed along a straight line for ZP response as well as PEE response. This means that the confidences for the fit of the regression equations to the observed values were >95% for all responses. Additionally, the randomly scatter pattern of the plot of residuals versus the predicted response (data not shown) indicated the models were adequate and did not show any violation of the independence or constant variance assumption [41].

As explained, the lack of fit test indicates the variation of data around the fitted model and determines if the selected model adequately represents the experimental data. In addition, the non-significant lack of fit shows the predictability of the model. As shown in Table insert in Fig. 2a, the lack of fit test for ZP was non-significant with $P > 0.05$ meaning that the selected model turned out to be adequate for the experimental data. The residual sum of squares is composed of a pure error component arising from the replicate runs at the center and a lack of fit component formed by pooling all the small effects and the removed interactions.

The relationship between the predicted and observed data was good, with R^2 0.968 and adjusted R^2_{adj} 0.965 indicating that the fitted model explains the 96.5% of the ZP variance. The difference between R^2_{adj} and R^2_{pred} (0.958) was <0.007, indicating they were in a good agreement.

Taking PEE into account, the lack of fit was also non-significant with $P > 0.05$ (Table insert in Fig. 2b) therefore, the model was adequate to fit the experimental data.

R^2 presented a value of 0.869 and $R^2_{adj} = 0.846$ was in a reasonable agreement with and $R^2_{pred} = 0.811$ (<0.2).

At the same time, relatively low values of the coefficients of variation obtained ($CV_{ZP} = 3.61$ and $CV_{PEE} = 4.14$) indicated a good precision and reliability of the experimental values. These findings are in accordance with Amini et al. [42].

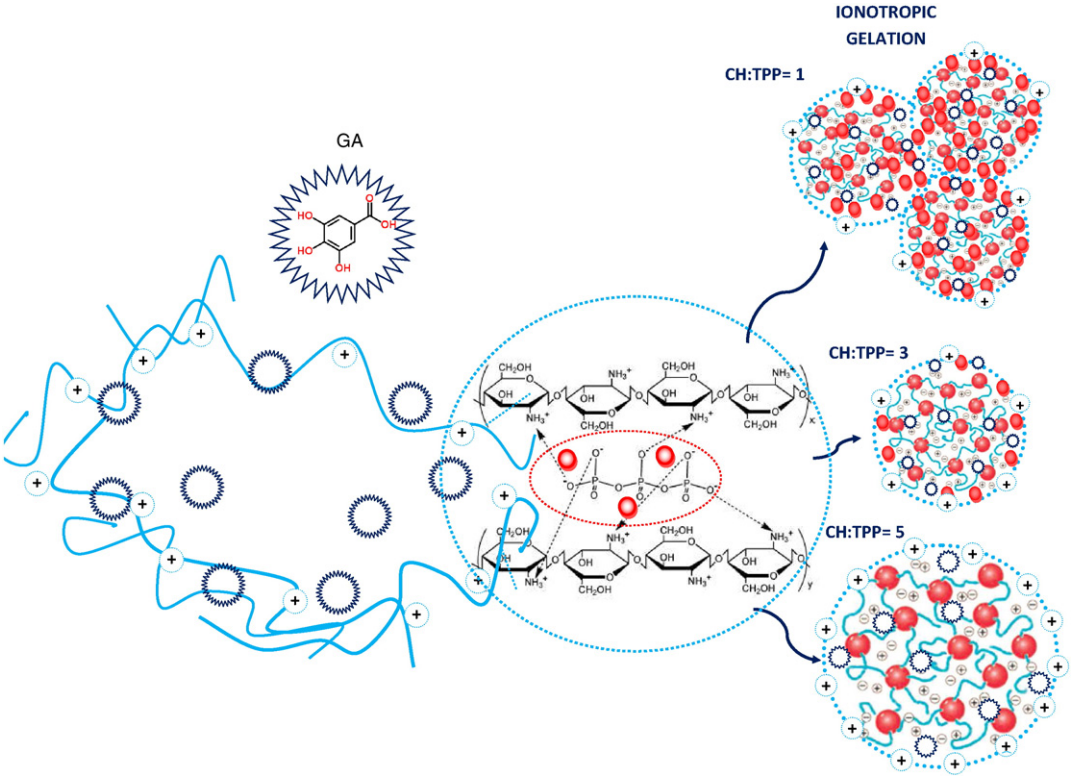

Fig. 4. Schematic representation of ionic crosslinking reaction between chitosan and TPP involved in the nanocomplex formulations. Influence of different CH:TPP ratios on ZP and particle sizes.

In summary, the regression models can be used to predict the response at any point in the space spanned by the factors in the design.

4.3. Global desirability

Modeling a measured response or a function of design variables implies to find areas where the process is likely to give desirable results. In many cases, the term desirable is a function of multiple responses.

According to Derringer and Suich [43], the general approach is convert each response *yi* into an individual desirability function d_i that varies over the range

$$0 \le d_i \le 1$$

with $d_i = 0$ representing a completely undesirable value of y_i and $d_i = 1$ representing a completely desirable or ideal response value. The mathematical model used to find a global desirability value, *D*, is the geometric media of individual desirability values [43], which gives

$$D = (d_1 \times d_2 \times \ldots\ldots d_m)^{1/m} \quad (9)$$

where there are *m* responses.

This transformation makes it possible to combine the results obtained for properties measured in different orders of magnitude. Thus, the simultaneous optimization process is used to find the levels of factors that demonstrate the maximum overall desirability [44].

Once the individual predictive equations were obtained (Eqs. (6) and (8)), two desirability functions were defined for the variables that were significantly affected by the formulation, that is, zeta potential and percentage encapsulation efficiency, where both responses were maximized.

Global overall desirability methodology was applied to find the optimum formulation that included 0.76% (w/w), CH:TPP ratio of 5 and 37 mg_{GA}/g_{CH} leading to values of +50 mV for ZP, 82% for PEE and 160 nm for nanoparticle diameter. The *D* value obtained turned out to be 0.934. The obtained value of desirability shows that the estimated function may represent the experimental model and desired conditions.

4.4. Optical characterization

The QuickScan technology was used to detect possible instability phenomena in the prepared systems, thus providing an accurate, qualitative description of the nanoparticle suspensions. As known, the occurrence of important transmission variation at the bottom and the top of the spectra indicates particle migration phenomena (clarification, sedimentation or creaming), while variations in the middle are related to changes in particle sizes [45]. According to Lorenzo et al. [46] this method was able to detect, at an early stage, the occurrence of different structural changes long before they could be observed by the naked-eye.

Fig. 3a and b depicts transmittance profiles of selected formulations as typical examples. Although the shape of the curves F_{11}, F_{15} and F_{12} was qualitatively similar they differed from each other with regard to the maximum transmittance reached (Fig. 3a). These values (0.01, 0.21 and 0.51) were related to the CH:TPP ratio (1, 3 and 5, respectively) since these formulations were prepared with the same CH and GA concentrations (0.75% and 50 mg/g_{CH}). On the other hand, high CH:TPP ratio combined with the lowest CH concentrations that led to the maximum CH amount free, produced practically transparent suspensions displaying the highest transmittance value (F_3, F_4 and F_9) while the transmittance fell to near zero when the ratio diminished to 1 and 1.81 and CH concentration was higher than 0.75% (w/w) (F_5, F_6 and F_{11}). According to Caddeo et al. [47] this fact highlights the important role chitosan plays in the structural organization of the nanosystems, consisting in an improvement of the stability. As described previously, the zeta potential is a useful tool to predict the sample stability by electrostatic repulsion. When the particles have a large negative or positive zeta potential, they remain separate each other and the suspension is stable as the case of sample F_{12} whose ZP value was about +46.6 mV. Considering particles with low zeta potential such as F_{11} (+5.3 mV on average), repulsive forces were small and the particles aggregated, resulting in suspension instability showing a transmittance value closer to zero. Therefore, it can be inferred that CH and TPP critically modified the sample stability through the modification of the surface charge of the system.

As can be observed in Fig. 3b, samples F_{13}, F_{14} and F_{15}, differing only in GA content (8, 92 and 50 mg/g_{CH}, respectively) presented similar transmittance value, about 0.22. This fact indicated that GA practically no had an influence on particle design parameters, in agreement with the findings obtained by means of response surface for ZP and PEE.

In addition, for samples F_9, F_{15} and F_{10} (Fig. 3b), with equal CH:TPP ratio (equal to 3) and GA concentration (50 mg/g_{CH}), the higher the CH concentration (0.3, 0.75 and 1.17%, respectively) was, the lower the transmittance value and hence the greater the turbidity value were.

In the same way, it could establish an inverse relationship between turbidity values obtained by means of Eq. (4) and both, transmittance values attained by QuickScan and ZP values (data not shown).

4.5. Particle diameter analysis

Chitosan's ability of quick gelling on contact with polyanions relies on the formation of inter- and intramolecular cross-linkages mediated by these counterions. As can be seen in the scheme presented in Fig. 4, CH-nanoparticles were obtained as a consequence of molecular linkages formed between TPP phosphates and chitosan amino group. Fig. 5a shows that the smallest particle diameters (ranged between 140 and

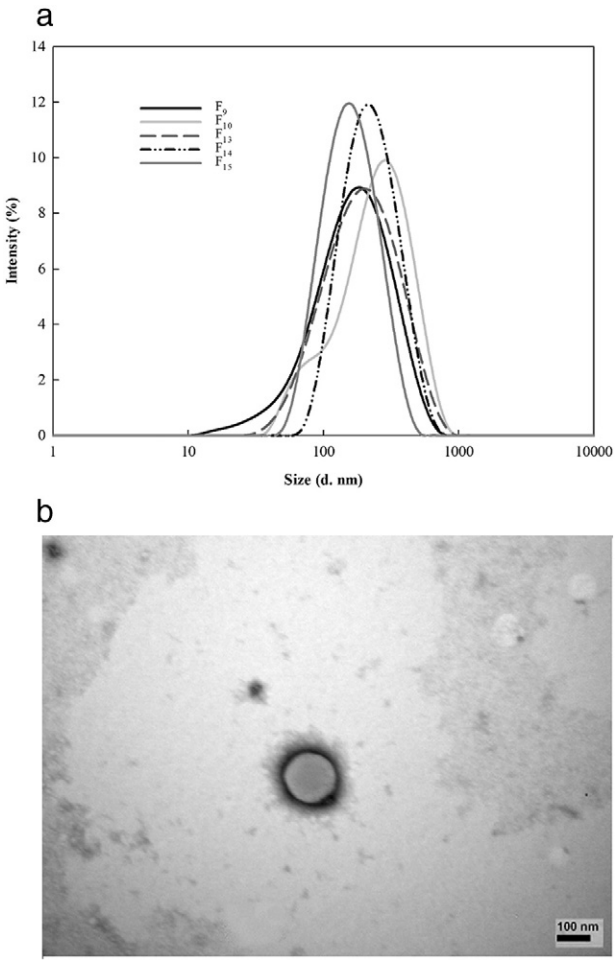

Fig 5. a) Size distribution of intensity of nanoparticles formulated with a common CH:TPP ratio of 3; b) TEM micrographs of gallic acid-loaded chitosan nanoparticles prepared using 0.75% CH, CH:TPP ratio of 3 and 50 mg_{GA}/g_{CH}.

188 nm on average) were obtained for the formulations F_9, F_{10}, F_{13}, F_{14} and F_{15}, which had in common the ratio CH:TPP equal to 3. They were stable as demonstrated by QuickScan method, but differed in the transmittance values which were 0.92, 0.04, 0.21, 0.22 and 0.21, respectively and had ZP values ranged between +22 and +30 mV.

On the other hand, particle diameters turned out to be higher than 700 nm for the formulations F_1, F_2, F_5, F_6 and F_{11}. Simultaneously, very low values of transmittance were obtained for these formulations prepared by the incorporation of the highest amount of TPP meaning the lowest CH:TPP ratios (1.81 and 1).

It was possible inferred that low values of transmittance could be obtained as a consequence of the formation of large particles as described in the preceding paragraph, or the presence of high amount of free CH in the suspension as in F_{10}.

It is worth noting that the highest CH concentration or the lowest CH:TPP ratio led to the instability of the system, with the achievement of large particles consistent with the lowest values of zeta potential. This was due to electrostatic interactions between the positive charge of chitosan polymer chains and negative charge of excess TPP leading to less positive surface charge of the particle.

Additionally, the PDI values obtained principally correlated with nanosize diameters. That is, PDI values lower than 0.3, observed for relatively monodisperse formulations, coincided with nanoparticle sizes about 160 nm on average and stable systems. Meanwhile, PDI values higher than 0.5 were associated with unstable systems and the highest diameters obtained for nanoparticles.

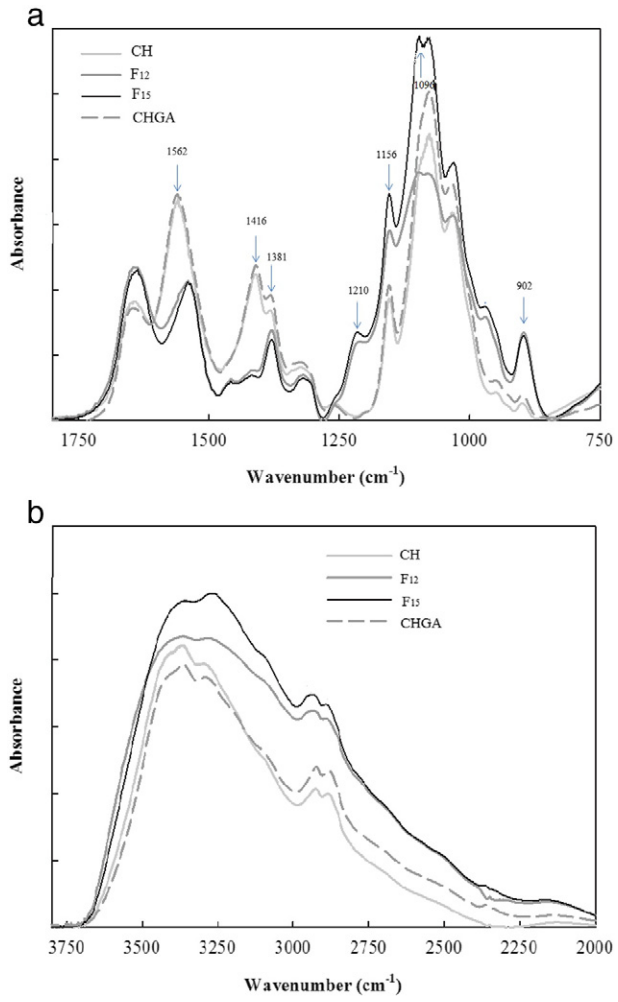

Fig. 6. FTIR spectra of CH, CHGA and CHTPP nanoparticles functionalized with GA films in: a) 1750–750 cm^{-1} and b) 3800–2000 cm^{-1} wavenumber regions.

The nanoparticles diameters could be confirmed by using TEM methodology as shown in Fig. 5b for the formulation F_{15}. The morphological analysis by TEM confirmed the nanosize of the formulation and indicated that the nanoparticles were roughly spherical in shape.

In summary, the most stable systems turned out to be those formulated with CH:TPP ratios equal to 3 and CH concentrations of approximately 0.75%, whose ZP values ranged between +22 and +30 mV. This fact correlated with the lowest nanoparticle diameters and PDI lower than 0.3. Bearing in mind these results and the above mentioned about ZP values in Section 4.2 (*Response Surface Methodology*), it could be inferred that the system stability not only depended on ZP value but also, and principally, on the CH:TPP ratio.

4.6. Chemical interactions of CH: TPP nanoparticles

To investigate CH–TPP nanoparticle formation, films of CH, CHGA and CH crosslinked with TPP were prepared as described in Section 3.7 (*FTIR spectroscopy*). Fig. 6a and b depicts FTIR spectra of CH nanoparticles (F_{12} and F_{15}), CH and CHGA. CH spectrum exhibited the characteristic absorption bands at 1644 cm^{-1} (C=O stretching in amide group, amide I vibration), 1562 cm^{-1} (–NH_2 bending in non-acetylated 2-aminoglucose primary amine) and 1381 cm^{-1} (C–O stretching of primary alcohol groups) (Fig. 6a). The absorption peak at 1156 cm^{-1} (antisymmetric stretching of the C–O–C glycosidic linkage between chitosan monomers) and 1033 cm^{-1} (skeletal vibrations involving the C–O stretching) typical of the chitosan saccharide structure were observed [48].

The presence of GA practically did not modify the CH spectrum, signal of that the interaction between CH and the active agent was not evident. According to Pasanphan et al. [49], a new significant peak at 1730 cm^{-1} would indicate ester linkage which was not observed in the present work probably because of the small amount of GA added (Fig. 6a). On the other hand, the nanoparticle spectra (F_{12} and F_{15}) involving CH, GA and the crosslinking agent TPP, showed evident difference compared to CH and CHGA spectra (Fig. 6a and b).

By observing FTIR spectra of crosslinked chitosan, the band at 1562 cm^{-1} underwent an absorbance reduction and a shift to 1536 cm^{-1} after the conjugation reaction with TPP creating ionic bonds. This fact could be attributed to the linkage between the phosphoric and ammonium ions. These interactions reduce CH solubility and are responsible for CH separation from the solution in the form of nanoparticles. The crosslinked chitosan also showed a peak for P=O at 1156 cm^{-1} [50].

According to Gierszewska-Drużyńska and Ostrowska-Czubenko [51] and Vimal et al. [52] the band at 1210 cm^{-1}, corresponding to P=O stretching, confirmed the formation of ionic crosslinks between NH_3^+ groups of chitosan and tripolyphosphate ions as observed in F_{12} and F_{15} spectra (Fig. 6a).

The other IR bands of TPP could be observed in F_{12} and F_{15} spectra such 1096 cm^{-1} (symmetric and antisymmetric stretching vibrations in PO_3 group) and 902 cm^{-1} (antisymmetric stretching of the P–O–P bridge) [53].

In all FTIR spectra, vibrations of hydroxyl and free amine groups, located in the region 3450–3250 cm^{-1}, were observed (Fig. 6b). This profile section experienced changes probably associated with the ionic crosslinking effect of TPP which resulted in the vibration mode change of the OH group and indicated a specific vibration of the NH group [54]. In accordance with the findings of Wu et al. [55], this region becomes wider, indicating that hydrogen bonding was enhanced (Fig. 6b).

As can be seen in Fig. 6a and b, the differences between FTIR spectra of F_{12} and F_{15} were basically linked to the intensity of TPP characteristic bands, given that the two formulations only differed in the CH:TPP ratio which were 5 and 3, respectively.

5. Conclusions

Chitosan-base nanoparticles loaded with gallic acid were successfully synthesized. The statistical experimental design methodology clearly

showed the feasibility of the optimization procedure in developing GA encapsulated nanoparticles. The design parameters of functionalized CH nanoparticles were optimized through a response surface method. Responses such as zeta potential and percentage encapsulation efficiency that permitted optimizing the system were dependent on the design parameters: chitosan concentration, CH:TPP ratio and GA concentration. Global desirability methodology was applied to find the optimum formulation that included 0.76% (w/w), CH:TPP ratio of 5 and 37 mg_{GA}/g_{CH} leading to ZP of +50 mV and 82% of PEE. TEM characterization revealed that the nanoparticles have a discrete spherical structure.

Additional analyses demonstrated that the most stable nanoparticle suspensions were achieved combining concentrations of chitosan ranging between 0.5 and 0.75% (w/w) with CH:TPP ratios higher than 3. These suspensions were characterized by their high stability confirmed through ZP and transmittance values which were higher than +25 mV and 0.21 on average, respectively as well as nanoparticle diameters of about 140 nm.

FTIR revealed the occurrence of both hydrogen bond and ionic interactions of CH-TPP which allowed the encapsulation and the improvement of the stability of the active agent.

Based on these findings, it can be concluded that the proposed nanoparticle formulations could be a potential candidate for the encapsulation and controlled release of active compounds such as gallic acid in order to be used for food preservation. In this sense, further studies are needed.

Acknowledgments

This work was supported by the Argentinean Agency for the Scientific and Technological Promotion (ANPCyT) (Project PICT 2012-0415) and the Argentinean National Research Council (CONICET) (PIP 2013-0109).

References

[1] S. Verma, A. Singh, A. Mishra, Gallic acid: molecular rival of cancer, Environ. Toxicol. Pharmacol. 35 (2013) 473–485.
[2] W. Pasanphan, S. Chirachanchai, Conjugation of gallic acid onto chitosan: an approach for green and water-based antioxidant, Carbohydr. Polym. 72 (2008) 169–177.
[3] S.B. Schreiber, J.J. Bozell, D.G. Hayes, S. Zivanovic, Introduction of primary antioxidant activity to chitosan for application as a multifunctional food packaging material, Food Hydrocoll. 33 (2013) 207–214.
[4] M. Xie, B. Hu, Y. Wang, X. Zeng, Grafting of gallic acid onto chitosan enhances antioxidant activities and alters rheological properties of the copolymer, J. Agric. Food Chem. 62 (2014) 9128–9136.
[5] K. Nagpal, S.K. Singh, D.N. Mishra, Nanoparticle mediated brain targeted delivery of gallic acid: in vivo behavioral and biochemical studies for improved antioxidant and antidepressant-like activity, Drug Deliv. 19 (8) (2012) 378–391.
[6] K. Konecsni, N.H. Low, M.T. Nickerson, Chitosan–tripolyphosphate submicron particles as the carrier of entrapped rutin, Food Chem. 134 (2012) 1775–1779.
[7] N. Atar, T. Eren, M.L. Yola, A molecular imprinted SPR biosensor for sensitive determination of citrinin in red yeast rice, Food Chem. 184 (2015) 7–11.
[8] T. Eren, N. Atar, M.L. Yola, H. Karimi-Maleh, A sensitive molecularly imprinted polymer based quartz crystal microbalance nanosensor for selective determination of lovastatin in red yeast rice, Food Chem. 185 (2015) 430–436.
[9] M.L. Yola, T. Eren, N. Atar, Molecular imprinted nanosensor based on surface plasmon resonance: application to the sensitive determination of amoxicillin, Sensors Actuators B Chem. 195 (2014) 28–35.
[10] A.P. Patel, Y. Hu, J.K. Tiwari, K.P. Velikov, Synthesis and characterization of zein-curcumin colloidal particles, Soft Matter 6 (2010) 6192–6199.
[11] A.C. Pinheiroa, A.I. Bourbona, M.A. Cerqueira, E. Maricato, C. Nunes, M.A. Coimbra, A.A. Vicente, Chitosan/fucoidan multilayer nanocapsules as a vehicle for controlled release of bioactive compounds, Carbohydr. Polym. 115 (2014) 1–9.
[12] H. Jonassen, A.-L. Kjøniksen, M. Hiorth, Stability of chitosan nanoparticles cross-linked with tripolyphosphate, Biomacromolecules 13 (2012) 3747–3756.
[13] Z. Teng, Y. Luo, Q. Wang, Carboxymethyl chitosan–soy protein complex nanoparticles for the encapsulation and controlled release of vitamin D3, Food Chem. 14 (2013) 524–532.
[14] S.A. Agnihotri, N.N. Mallikarjuna, T.M. Aminabhavi, Recent advances on chitosan-based micro- and nanoparticles in drug delivery, J. Control. Release 100 (2004) 5–28.
[15] A. Alishahi, A. Mirvaghefi, M.R. Tehrani, H. Farahmand, S.A. Shojaosadati, F.A. Dorkoosh, M.Z. Elsabee, Shelf life and delivery enhancement of vitamin C using chitosan nanoparticles, Food Chem. 126 (2011) 935–940.
[16] Y.C. Luo, B.C. Zhang, W.H. Cheng, Q. Wang, Preparation, characterization and evaluation of selenite-loaded chitosan/TPP nanoparticles with or without zein coatin, Carbohydr. Polym. 82 (2010) 942–951.
[17] D.-W. Tang, S.-H. Yu, Y.-C. Ho, B.-Q. Huang, G.-J. Tsai, H.-Y. Hsieh, H.-W. Sung, F.-L. Mi, Characterization of tea catechins-loaded nanoparticles prepared from chitosan and an edible polypeptide, Food Hydrocoll. 30 (2012) 33–41.
[18] S.A. Papadimitriou, D.S. Achilias, D.N. Bikiaris, Chitosan-g-PEG nanoparticles ionically crosslinked with poly(glutamic acid) and tripolyphosphate as protein delivery systems, Int. J. Pharm. 430 (2012) 318–327.
[19] S. Honary, P. Ebrahimi, R. Hadianamrei, Optimization of particle size and encapsulation efficiency of vancomycin nanoparticles by response surface methodology, Pharm. Dev. Technol. 19 (8) (2014) 987–998.
[20] M. Homayoonfal, F. Khodaiyan, M. Mousavi, Modelling and optimising of physicochemical features of walnut-oil beverage emulsions by implementation of response surface methodology: effect of preparation conditions on emulsion stability, Food Chem. 174 (2015) 649–659.
[21] K.A. Kishore, G.V. Reddy, Statistical design and optimization of metal ion concentrations for submerged fermentation of citric acid, Sci. Rev. Chem. Commun. 2 (2012) 66–75.
[22] S.M. Ghoreishi, M. Behpour, A. Khoobi, Central composite rotatable design in the development of a new method for optimization, voltammetric determination and electrochemical behavior of betaxolol in the presence of acetaminophen based on a gold nanoparticle modified electrode, Anal. Methods 4 (2012) 2475–2485.
[23] J. Zhang, Y. Fan, E. Smith, Experimental design for the optimization of lipid nanoparticles, J. Pharm. Sci. 98 (2009) 1813–1819.
[24] N.A. Amenaghawon, S.E. Ogbeide, C.O. Okieimen, Application of statistical experimental design for the optimisation of dilute sulphuric acid hydrolysis of cassava bagasse, Acta Polytech. Hung. 11 (2014) 239–250.
[25] F.A. Fiorda, M.S. Soares Jr., F.A. da Silva, C.mM.A. de Moura, M.V.E. Grossmann, Physical quality of snacks and technological properties of pre-gelatinized flours formulated with cassava starch and dehydrated cassava bagasse as a function of extrusion variables, LWT Food Sci. Technol. 62 (2015) 1112–1119.
[26] P. Calvo, R.C. López, J.L. Vila-Jato, M.J. Alonso, Novel hydrophilic chitosan–polyethylene oxide nanoparticles as protein carriers, J. Appl. Polym. Sci. 63 (1997) 125–132.
[27] M. Gaumet, A. Vargas, R. Gurny, F. Delie, Nanoparticles for drug delivery: the need for precision in reporting particle size parameters, Eur. J. Pharm. Biopharm. 69 (2008) 1–9.
[28] S.K. Janardhanan, I. Ramasamy, B.U. Nair, Synthesis of iron oxide nanoparticles using chitosan and starch templates, Transit. Met. Chem. 33 (2008) 127–131.
[29] G.E.P. Box, J.S. Hunter, W.G. Hunter, Statistics for Experimenters: Design, Innovation, and Discovery, second ed. John Wiley & Sons, Inc., Hoboken, New Jersey, 2005.
[30] R.H. Myers, D.C. Montgomery, C.M. Anderson-Cook, Response Surface Methodology in Process and Product Optimization Using Designed Experiments, third ed. John Wiley & Sons, Inc., Hoboken, New Jersey, 2009.
[31] M.S. Alvarez Cerimedo, C. Huck Iriart, R. Candal, M.L. Herrera, Stability of emulsions formulated with high concentrations of sodium-caseinate and trehalose, Food Res. Int. 43 (2010) 1482–1493.
[32] N.A. Camino, A.M.R. Pilosof, Hydroxypropylmethylcellulose at the oil-water interface. Part II. Submicron-emulsions as affected by pH, Food Hydrocoll. 25 (2011) 1051–1062.
[33] D.H. Melik, H.S. Fogler, Turbidimetric determination of particle size distributions of colloidal systems, J. Colloid Interface Sci. 92 (1982) 161–179.
[34] Q. Gan, T. Wang, C. Cochrane, P. McCarron, Modulation of surface charge, particle size and morphological properties of chitosan–TPP nanoparticles intended for gene delivery, Colloids Surf. B: Biointerfaces 44 (2005) 65–73.
[35] M.S. Bitaraf, F. Khodaiyan, M.A. Mohammadifar, S.M. Mousavi, Application of response surface methodology to improve fermentation time and rheological properties of probiotic yogurt containing *Lactobacillus reuteri*, Food Bioprocess Technol. 5 (2012) 1394–1401.
[36] E. Ramadan, T. Borg, G.M. Abdelghani, N.M. Saleh, Transdermal microneedle-mediated delivery of polymeric lamivudine-loaded nanoparticles, J. Pharm. Technol. Drug Res. 5 (2016) 1.
[37] S. Honary, F. Zahir, Effect of zeta potential on the properties of nano-drug delivery systems - a review (part 2), Trop. J. Pharm. Res. 12 (2013) 265–273.
[38] R. Prabhat, L. Mishra, b. Al Shaal, R.H. Müller, C.M. Keck, Production and characterization of Hesperetin nanosuspensions for dermal delivery, Int. J. Pharm. 371 (2009) 182–189.
[39] M.A. Kalama, A.A. Khana, S. Khana, A. Almalik, Optimizing indomethacin-loaded chitosan nanoparticle size,encapsulation, and release using Box–Behnken experimental design, Int. J. Biol. Macromol. 87 (2016) 329–340.
[40] D. Xu, Z. Aihemaiti, Y. Cao, C. Teng, X. Li, Physicochemical stability, microrheological properties and microstructure of lutein emulsions stabilized by multilayer membranes consisting of whey protein isolate, flaxseed gum and chitosan, Food Chem. 202 (2016) 156–164.
[41] K.M. Lee, S.B.A. Hamid, Simple response surface methodology: investigation on advance photocatalytic oxidation of 4-chlorophenoxyacetic acid using UV-active ZnO photocatalyst, Materials 8 (2015) 339–354.
[42] M. Amini, H. Younesi, N. Bahramifar, A.A.Z. Lorestani, F. Ghorbani, A. Daneshi, M. Sharifzadeh, Application of response surface methodology for optimization of lead biosorption in an aqueous solution by *Aspergillus niger*, J. Hazard. Mater. 154 (2008) 694–702.
[43] G.C. Derringer, R. Suich, Simultaneous optimization of several response variables, J. Qual. Technol. 12 (1980) 214–219.
[44] M.A. Bezerra, R.E. Santelli, E.P. Oliveira, L.S. Villar, L.A. Escaleira, Response surface methodology (RSM) as a tool for optimization in analytical chemistry: a review, Talanta 76 (2008) 965–977.
[45] C. Carbone, A. Campisi, D. Manno, A. Serra, M. Spatuzza, T. Musumeci, R. Bonfanti, G. Puglisi, The critical role of didodecyldimethylammonium bromide on physicochemical, technological and biological properties of NLC, Colloids Surf. B: Biointerfaces 121 (2014) 1–10.

[46] G. Lorenzo, N. Zaritzky, A. Califano, Mechanical and optical characterization of gelled matrices during storage, Carbohydr. Polym. 117 (2015) 825–835.
[47] C. Caddeo, O. Díez-Sales, R. Pons, C. Carbone, G. Ennas, G. Puglisi, A.M. Fadda, M. Manconi, Cross-linked chitosan/liposome hybrid system for the intestinal delivery of quercetin, J. Colloid Interface Sci. 461 (2016) 69–78.
[48] S. Rivero, M.A. García, A. Pinotti, Crosslinking capacity of tannic acid in plasticized chitosan films, Carbohydr. Polym. 82 (2010) 270–276.
[49] W. Pasanphan, R. Buettner Garry, S. Chirachanchai, Chitosan gallate as a novel potential polysaccharide antioxidant: an EPR stud, Carbohydr. Res. 345 (2010) 132–140.
[50] D.R. Bhumkar, V.B. Pokharkar, Studies on effect of pH on cross-linking of chitosan with sodium tripolyphosphate: a technical note, AAPS Pharm. Sci. Tech. 7 (2006) E1–E6.
[51] M. Gierszewska-Drużyńska, J. Ostrowska-Czubenko, Influence of crosslinking process conditions on molecular and supermolecular structure of chitosan hydrogel membrane, Progress on Chemistry and Application of Chitin and Its Derivatives. Polish Chitin Society, vol. XVI, Media-Press, Lodz, Poland 2011, pp. 15–22.
[52] S. Vimal, S. Abdul Majeed, G. Taju, K.S. Nambi, N. Sundar Raj, N. Madan, M.A. Farook, T. Rajkumar, D. Gopinath, A.S. Sahul Hameed, Chitosan tripolyphosphate (CS/TPP) nanoparticles: preparation, characterization and application for gene delivery in shrimp, Acta Trop. 128 (2013) 486–493.
[53] M. Gierszewska-Drużyńska, J. Ostrowska-Czubenko, The effect of ionic crosslinking thermal properties of hydrogel chitosan membranes, Progress on Chemistry and Application of Chitin and Its Derivatives. Polish Chitin Society, vol. XV, Media-Press, Lodz, Poland 2010, pp. 25–32.
[54] A.L. Holanda, M.V.L. Fook, R. Swarnakar, Preparation and characterization of chitosan-insulin-tripolyphosphate membrane for controlled drug release: effect of cross linking agent, J. Biomed. Nanotechnol. 5 (2014) 211–219.
[55] Y. Wu, W. Yang, C. Wang, J. Hu, S. Fu, Chitosan nanoparticles as a novel delivery system for ammonium glycyrrhizinate, Pharm. Nanotechnol. 295 (2005) 235–245.